Materials Today Bio 24 (2024) 100941

Contents lists available at ScienceDirect

Materials Today Bio

journal homepage: www.journals.elsevier.com/materials-today-bio

Cancer cell membrane-camouflaged CuPt nanoalloy boosts chemotherapy of cisplatin prodrug to enhance anticancer effect and reverse cisplatin resistance of tumor

Yuehao Gan [a,b,1], Wenteng Xie [b,c,1], Miaomiao Wang [a,b,1], Peng Wang [a], Qingdong Li [a], Junjie Cheng [c], Miao Yan [a], Jikai Xia [d,***], Zhengyan Wu [b,**], Guilong Zhang [a,*]

[a] School of Pharmacy, Shandong Technology Innovation Center of Molecular Targeting and Intelligent Diagnosis and Treatment, Binzhou Medical University, Yantai, 264003, PR China
[b] Key Laboratory of High Magnetic Field and Ion Beam Physical Biology, Hefei Institutes of Physical Science, Chinese Academy of Sciences, Hefei, 230031, PR China
[c] Engineering and Materials Science Experiment Center, University of Science and Technology of China, Hefei, 230026, PR China
[d] Department of Radiology, Yantai Affiliated Hospital of Binzhou Medical University, Yantai, 264100, Shandong, PR China

ARTICLE INFO

Keywords:
CuPt nanoalloy
ROS production
GSH depletion
Hypoxia relief
Reversing tumor resistance

ABSTRACT

The biotoxicity and chemotherapeutic resistance of cisplatin (CDDP) pose a challenge for tumor therapy. Practically, the change in the therapeutic response of tumor from resistance to sensitivity are impressive but challenging. To this end, we propose a strategy of "one stone, three birds" by designing a CuPt nanoalloy to simultaneously eliminate GSH, relieve hypoxia, and promote ROS production for effectively reversing the platinum (IV) (Pt(IV), (c,c,t-[Pt(NH_3)$_2$Cl$_2$(OOCCH$_2$CH$_2$COOH)$_2$)) resistance. Notably, the CuPt nanoalloy exhibits ternary catalytic capabilities including mimicking GSH oxidase, catalase and peroxidase. With the subsequent disguise of tumor cell membrane, the CuPt nanoalloy is conferred with homologous targeting ability, making it actively recognize tumor cells and then effectively internalized by tumor cells. Upon entering tumor cell, it gives rise to GSH depletion, hypoxia relief, and oxidative stress enhancement by catalyzing the reaction of GSH and H_2O_2, which mitigates the vicious milieu and ultimately reinforces the tumor response to Pt(IV) treatment. *In vivo* results prove that combination therapy of mCuPt and Pt(IV) realizes the most significant suppression on A549 cisplatin-resistant tumor. This study provides a potential strategy to design novel nanozyme for conquering resistant tumor.

1. Introduction

Cisplatin (CDDP), as a clinical first-line drug, has shown great application for broad-spectrum tumor treatment (i.e. breast cancer, gastric cancer, lung cancer, etc.), and it significantly enhanced the five-year survival rate of patients [1–3]. However, the acquired drug resistance and systemic toxicity of CDDP severely compromise its anticancer effect, resulting in a poor prognosis [4–6]. Compared to CDDP, the platinum(IV) (Pt (IV), (c,c,t-[Pt(NH_3)$_2$Cl$_2$(OOCCH$_2$CH$_2$COOH)$_2$)) prodrug with two axial ligands can specifically respond to tumor cells, which is converted into cytotoxic CDDP by excessive glutathione (GSH) in tumor cells, contributing to chemotherapy [7–9]. Despite its advantages, Pt (IV) prodrug still exhibits weak anticancer activity in suppressing tumor growth, limiting its clinical application [10]. One reason for this is that cellular CDDP easily binds with GSH, forming GS-Pt adduct, which can be expelled from cancer cells through ATP-dependent glutathione S-conjugate pumps, leading to the inactivation of CDDP [11,12]. Additionally, hypoxia caused by abnormal blood vessels and metabolic changes in tumors results in the accumulation of nucleophilic substances that can attack and deactivate CDDP [13,14]. Considering these factors, depleting GSH and simultaneously increasing the oxygen level in tumors could potentially improve the

* Corresponding author.
** Corresponding author.
*** Corresponding author.
E-mail addresses: myxjk@sina.com (J. Xia), zywu@ipp.ac.cn (Z. Wu), glzhang@bzmc.edu.cn (G. Zhang).
[1] These authors contributed equally to this work.

https://doi.org/10.1016/j.mtbio.2023.100941
Received 4 October 2023; Received in revised form 2 December 2023; Accepted 30 December 2023
Available online 2 January 2024

antitumor effect of Pt(IV) prodrug.

Catalytic therapy can effectively disrupt the balance of cellular redox and induce tumor cell death by modulating intracellular substances such as acidity, GSH, and other biomolecules [15–17]. Nanozymes, which possess comparable catalytic capability and kinetics to natural enzymes, as well as superior stability and accessibility, have garnered attention in biomedicine [18,19]. Numerous efforts have been dedicated to developing versatile and intricate nanozymes for tumor eradication [20–22]. For instance, nanozymes with peroxidase (POD)-like activity and GSH oxidase (GSHOx)-like activity can promote the production of •OH and reduce the content of GSH in cancer cells, thereby enhancing ROS production and amplifying oxidative stress [23,24]. However, these nanozymes lack sufficient bioavailability and potency since they are substance-selective rather than tumor-selective. Consequently, conventional nanozymes cannot guarantee effective dosage in tumors or safe concentration in normal tissues [25]. Therefore, it is necessary to develop tumor-selective and tumor-specific nanozymes through rational design and functionalization. Strategies such as conjugating tumor affinity ligands into nanozymes and coating cell membranes onto nanozymes have been proposed to improve their targeting ability [26,27]. Among these, modifying homogeneous cancer cell membranes may be a universal and feasible approach to enhance the specificity of nanozymes considering the limited number of identified tumor receptors. Copper-based nanozymes have recently attracted significant interest in cancer therapy due to their superior GSHOx-like and POD-like activity, while bimetallic nanoparticles based on platinum (Pt) have been found to exhibit higher catalytic activity than mono-metallic catalysts due to their high charge-transfer efficiency [28–31]. For instance, $PtCu_3$ alloy demonstrated stronger catalytic activity compared to elemental copper nanoparticles and showed excellent anticancer activity [32,33]. Moreover, the CAT-like activity of $PtCu_3$ alloy can overcome the hypoxic restriction in tumor treatment. Therefore, combining CuPt alloy with platinum prodrug may be an effective approach to reverse drug resistance and enhance antineoplastic activity through the synergistic action of ROS damage and chemotherapy.

In this study, we developed a tumor cell membrane-camouflaged CuPt nanozyme (mCuPt) with triple enzyme-mimetic activity (CAT, POD, and GSHOx) to reverse cisplatin resistance via tuning the tumor microenvironment and restoring the chemotherapeutic effect of Pt(IV) prodrug (Scheme 1). The mCuPt nanozyme actively recognized and accumulated in tumors through homotypic targeting. Once internalized by tumor cells, the mCuPt nanozyme catalyzed the conversion of endogenous H_2O_2 into •OH and O_2, and depleted intracellular GSH. This simultaneous action relieved tumor hypoxia and increased oxidative stress. The excessive ROS induced mitochondrial dysfunction, leading to reduced cellular ATP supply and decreased cisplatin excretion, ultimately reversing cisplatin resistance. By combining mCuPt with Pt(IV) prodrug, we effectively modulated the tumor microenvironment, making the tumor susceptible to Pt(IV) and overcoming cisplatin resistance. This work presents a promising biomimetic nanozyme as a chemotherapy-reactivated adjuvant for reversing cisplatin resistance in tumors.

2. Results and discussion

2.1. Preparation and characterization of CuPt nanoalloy

The CuPt nanoalloy was synthesized using a microwave-assisted method. Initially, $Pt(acac)_2$, $Cu(acac)_2$, and polyvinylpyrrolidone dissolved in diethylene glycol were transferred into a microwave reaction

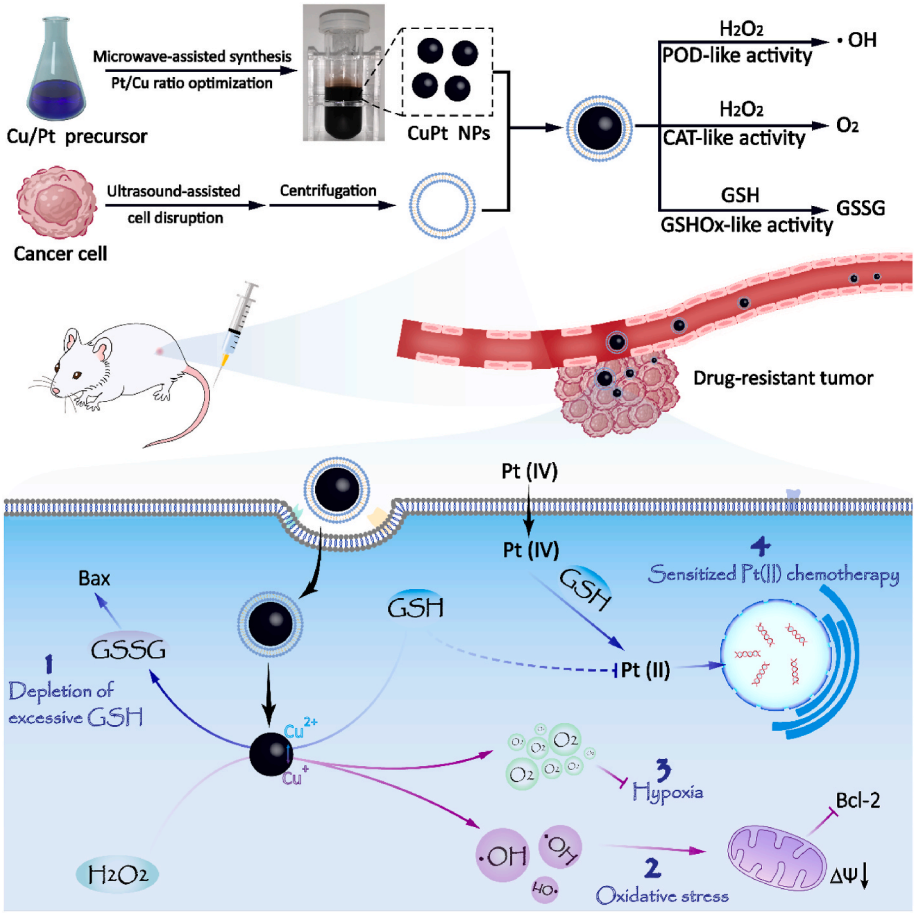

Scheme 1. Schematic illustration of fabrication and the synergistic antineoplastic process of mCuPt.

system and heated at 240 °C for 15 min. Subsequently, a black product was obtained (inset of Fig. 1a). In comparison to conventional solvothermal synthesis [32,33], the syntheses presented here are more efficient, time-saving, and high-performing. Given the interdependence of composition, structure, and function of nanozymes [34], we investigated the impact of the Pt/Cu ratio on the morphology and size of the nanoalloy. Five samples were synthesized with Pt/Cu molar ratios ranging from 1.7 % to 38 % and labeled as CuPt-1 to CuPt-5, respectively (Fig. S1). CuPt-1 exhibited irregular morphology with a size of approximately 100 nm. In contrast, CuPt-2 and CuPt-3 displayed uniform size and shape, making them suitable for *in vivo* applications. However, when the Pt content increased, the structures of CuPt-4 and CuPt-5 were significantly disrupted, indicating that excessive Pt atoms hindered the formation of the CuPt nanoalloy. Furthermore, we investigated the catalytic performance of these nanoalloys. As illustrated in Fig. S2, the POD-like and CAT-like activities of the CuPt nanoalloy increased significantly with increasing Pt content, while the GSHOx-like activity gradually decreased. This result suggests that the consumption of GSH might be medicated by oxidation of Cu^{2+}. Considering the POD-like, CAT-like, and GSHOx-like activities, as well as the structure of the CuPt nanoalloy, we selected CuPt-3 for further investigation, denoted as CuPt nanoalloy hereafter.

It could be seen from Fig. 1a–c that CuPt exhibited a spherical shape with a diameter of 29.5 nm, whereas a slight increment of hydrodynamic diameter (44 nm) corresponded well with TEM results (Fig. S3). Additionally, high-resolution TEM (HRTEM) image revealed an interplanar spacing of 0.22 nm in the CuPt nanoalloy, consistent with the (1 1 1) plane (inset of Fig. 1b). Element mapping and energy dispersive spectroscopy (EDS) results confirmed the uniform distribution of Cu and Pt elements in the nanoalloy, with a Pt/Cu atom ratio of approximately 12 %, which closely matched the inductively coupled plasma (ICP) results (Fig. 1d and e). Furthermore, X-ray diffraction (XRD) and X-ray photoelectron spectroscopy (XPS) were employed to analyze the crystal structure and element valence of the CuPt nanoalloy (Fig. 1f–i). The XRD pattern of CuPt closely matched the standard cards of Cu (JPCD 01–1241) and CuPt (JPCD 35–1358). Moreover, the predominant crystal phase of the CuPt nanoalloy was attributed to elemental copper, likely due to the low Pt content in the nanoalloy. The full XPS spectrum revealed characteristic peaks of Cu, Pt, C, N, and O. The Cu2p XPS spectrum of CuPt displayed two peaks at 931.2 eV and 950.88 eV, corresponding to Cu^0 2p3/2 and Cu^0 2p1/2, respectively. The Pt4f XPS spectrum was deconvoluted to three peaks at 69.9 eV, 73.3 eV, and 75.58 eV, corresponding to Pt^0 4f5/2, Pt^0 4f7/2, and Pt^{4+} 4f7/2, respectively. Collectively, these results confirm the successful fabrication of the CuPt nanoalloy with a size of 29.5 nm.

2.2. Enzymatic activity of CuPt nanozymes

Then, the ternary catalytic activities of CuPt in aqueous solutions were sequentially examined using colorimetric assay and dissolved oxygen determination (Fig. 2a). The •OH production catalyzed by CuPt was trapped using 5,5-dimethyl-1-pyrroline N-oxide (DMPO) and measured using an electron paramagnetic resonance (EPR) detector. The results exhibited a significant 1:2:2:1 characteristic peak (Fig. 2b),

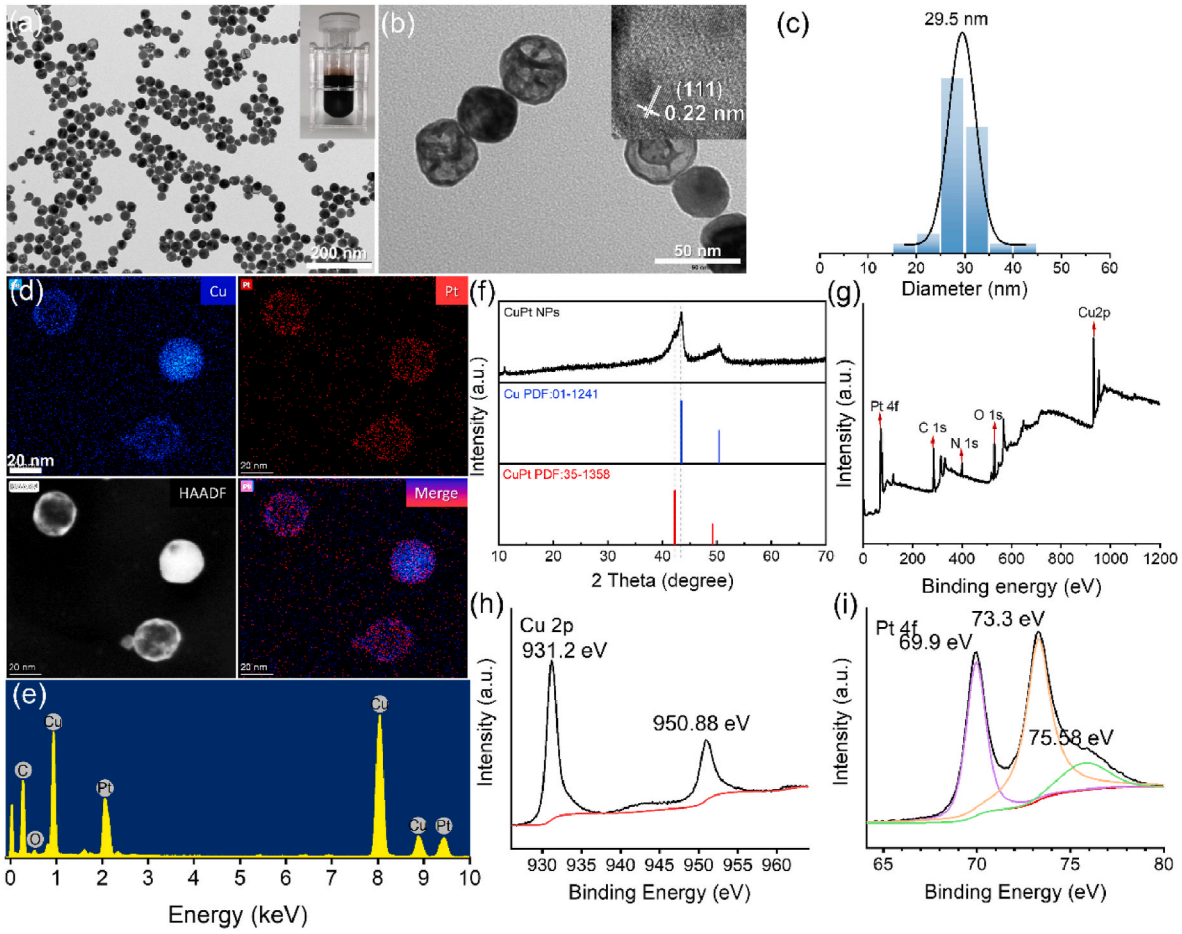

Fig. 1. Physiochemical characterization of CuPt nanoalloys. (a) Low-magnification TEM image of CuPt (inset: digital graph of CuPt in microwave tube); (b) High-magnification TEM image of CuPt (inset: HRTEM images); (c) Actual size distribution obtained from TEM image; (d) High-angle annular dark field image and elemental mapping and (e) EDS spectrum of CuPt; (f) XRD pattern of CuPt; (g) XPS full spectrum and (h) Cu2p spectrum and (i) Pt4f spectrum of CuPt.

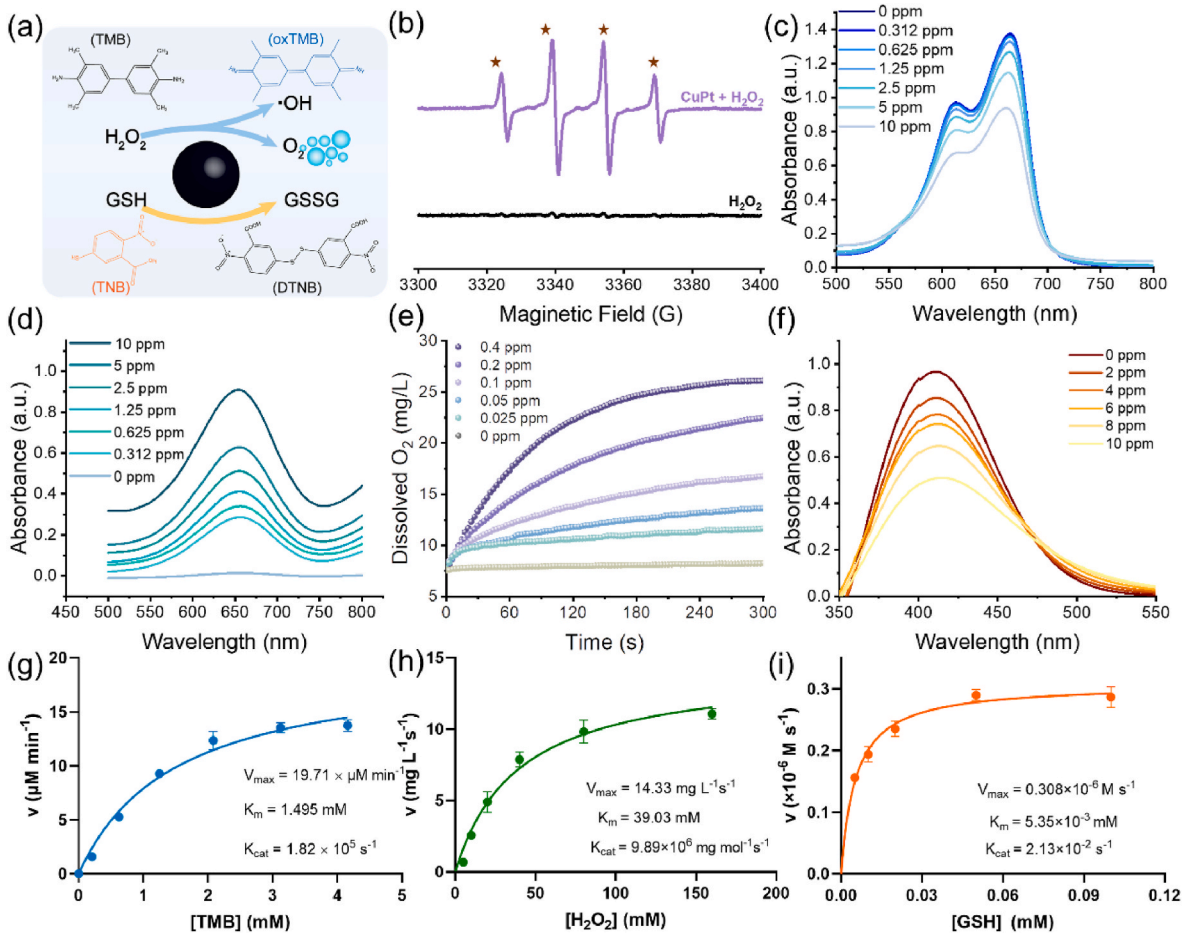

Fig. 2. *In vitro* ternary enzyme-like catalytic performance. (a) Diagram for CuPt catalyzed H_2O_2 into •OH and O_2 and depleted GSH; (b) ESR spectrum of •OH generation; the •OH detection using UV–vis spectrum of catalyzed oxidation of (c) MB degradation and (d) TMB color; (e) O_2 production detection by dissolved O_2 meter; (f) GSH depletion detection using UV–vis spectrum of DTNB/GSH adducts; Enzymatic kinetic analysis of (g) POD-like activity, (h) CAT-like activity and (i) GSHOx-like activity. (For interpretation of the references to colour in this figure legend, the reader is referred to the Web version of this article.)

indicating strong POD-like activity. Subsequently, methylene blue (MB) and 3,3′,5,5′-tetramethylbenzidine (TMB)were employed as peroxidase substrates to semi-quantitatively evaluate the POD-like activity of CuPt (Fig. 2c and d). The results indicated that the absorbance of oxidized TMB gradually enhanced with the increase of CuPt, and the MB absorbance gradually weakened, demonstrating concentration-dependent POD-like activity. The fitting curve of reaction velocity and H_2O_2 concentration conformed to the typical Michaelis-Menten equation, and the corresponding Michaelis constant (K_m), maximal reaction velocity (V_{max}) and catalytic constant (K_{cat}) values of CuPt were calculated to be 19.71 μM s^{-1}, 1.495 mM and 1.82 × 10^5 s^{-1}, respectively (Fig. 2g; S4a and S4b), which was significantly higher than classical POD-like nanozyme [35,36]. Furthermore, the CAT-like activity of CuPt was also investigated by measuring the dissolved oxygen in the H_2O_2 aqueous solution. As displayed in Fig. 2e, the output of dissolved oxygen significantly raised after CuPt treatment and displayed a concentration-dependent manner. The CAT-like enzyme kinetic parameters of CuPt were also determined by fitting the Michaelis-Menten equation (Fig. 2h and Fig. S4c). Interestingly, the CuPt nanoalloy exhibited higher CAT-like activity compared to pure Pt nanoparticles [33]. Additionally, besides its action on H_2O_2, CuPt also released Cu^{2+} under mild acidity which could oxidize GSH (Fig. S5). Simultaneously, the reduced Cu^+ product participated in POD-mimic catalysis. The DTNB probe was employed to detect residual GSH using UV–vis spectra at a wavelength of 412 nm. It was observed that the ability of CuPt to deplete GSH was concentration-dependent (Fig. 2f). Similarly, the GSHOx-like enzymatic parameters of CuPt were also investigated and presented in Fig. 2i and Fig. S4d. Consequently, we concluded that CuPt downregulated GSH while simultaneously enhancing the generation of •OH and O_2 through these cascaded catalytic reactions, thereby amplifying intracellular oxidative stress and relieving hypoxia.

2.3. Fabrication and characterization of cancer cell membrane camouflaged nanozyme

Prior to assessing cytotoxicity and tumor suppression, it is important to optimize the targeting ability and biocompatibility of CuPt nanoalloy. Previous studies have shown that nanoparticles ranging from 20 to 200 nm can passively target tumors through the enhanced permeability and retention (EPR) effect. However, this targeting efficiency is too low to effectively act at the tumor site and achieve the desired anticancer effect. Recent research has discovered that nanoparticles enveloped in tumor cell membranes can effectively target homologous tumors and promote the internalization of nanoparticles by tumor cells. In this study, the CuPt nanoalloy was camouflaged with two types of homologous cancer cell membranes derived from A549R cancer cells and 4T1 cancer cells, respectively (Fig. 3a). TEM images clearly showed a low-contrast superficial layer on the surface of the CuPt nanoalloy after being coated with A549R membrane (mCuPt A549R), with the A549R membrane thickness measuring approximately 2 nm (Fig. 3b). Similar results were observed with the 4T1 cell membrane coated CuPt (mCuPt 4T1) (Fig. 3c). Compared to CuPt, the hydrodynamic size of mCuPt

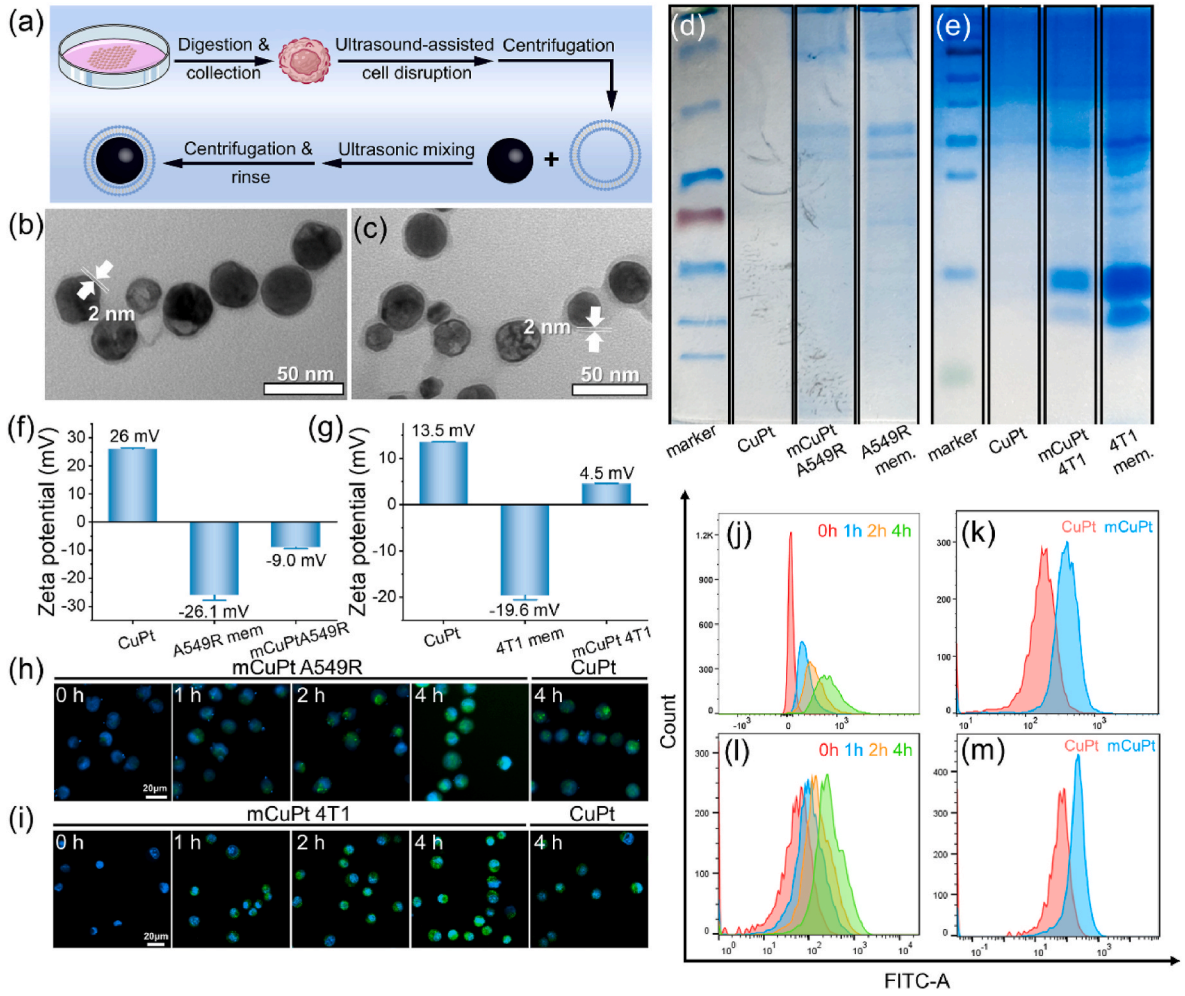

Fig. 3. (a) Diagram for fabrication process of cancer cell membrane-cloaked CuPt; TEM images of (b) mCuPt A549R and (c) mCuPt 4T1; SDS-PAGE protein analysis of (d) mCuPt A549R and (e) mCuPt 4T1; Zeta potential analysis of (f) mCuPt A549R and (g) mCuPt 4T1; CLSM observation for cell internalization of (h) mCuPt A549R and (i) mCuPt 4T1 at different time points; Flow cytometry for cell internalization of (j, k) mCuPt A549R and (l, m) mCuPt 4T1.

A549R and mCuPt 4T1 significantly increased (Fig. S6), and the zeta potentials dramatically decreased (Fig. 3f and g), indicating successful coating of the cancer cell membrane onto the surface of the CuPt nanoalloy. To further confirm the successful fabrication of mCuPt, SDS-polyacrylamide gel electrophoresis (SDS-PAGE) was conducted. It could be seen in Fig. 3d and e that mCuPt A549R and mCuPt 4T1 exhibited similar protein bands to A549 and 4T1 cell membranes, further confirming successful fabrication of mCuPt. Subsequently, the colloidal stability of mCuPt A549R and mCuPt 4T1 was studied under different media (FBS and 1640 culture medium) (Fig. S7 and Fig. S8). The DLS results showed a slight decrease in hydrodynamic size after standing for 48 h, and TEM observation demonstrated no significant aggregation or decomposition in the morphology of mCuPt. These results indicated excellent colloidal stability of mCuPt. Additionally, the cytotoxicity of mCuPt towards L929 cells was explored using the MTT assay, which revealed benign biocompatibility of mCuPt towards normal cells (Fig. S9). The homologous targeting abilities of mCuPt A549R and mCuPt 4T1 were then assessed by observing their cell internalization level using CLSM and flow cytometry analysis. As shown in Fig. 3h, 3i, 3j and 3l, the internalization process of mCuPt A549R and mCuPt 4T1 by A549 cells and 4T1 cells was time-dependent. Furthermore, the uptake of mCuPt A549R and mCuPt 4T1 was significantly higher than that of CuPt (Fig. 3kand 3m). Based on the mentioned analysis, it was concluded that coating the CuPt nanoalloy with cancer cell membranes can effectively enhance cell uptake of the nanoalloys, demonstrating excellent tumor-targeting ability. In order to explore the internalization pathway of mCuPt, the mCuPt-treated 4T1 cells were co-incubated with 4 °C, chlorpromazine, and amiloride, respectively. As shown in Fig. S10, the fluorescence intensity of A549R cells treated with mCuPt plus 4 °C remarkably decreased, moreover the use of endocytosis inhibitors including chlorpromazine and amiloride decreased cellular green fluorescence at the different degrees. These results suggested that internalization of mCuPt depended on energy-mediated endocytosis.

2.4. *In vitro antitumor activity of mCuPt-sensitized chemotherapy*

After entering into cancer cells, we assessed the anticancer activity of mCuPt and its chemosensitization action to reverse cisplatin resistance *in vitro*. Initially, the viability of 4T1 cells treated with CuPt and mCuPt 4T1 gradually decreased as the concentration increased, indicating a dose-dependent manner (Fig. 4a). Moreover, mCuPt 4T1 exhibited slightly stronger inhibition of cell viability than CuPt, which was attributed to its homologous targeting ability. Notably, the combination of Pt(IV) and mCuPt 4T1 (10 μg/mL) significantly enhanced 4T1 cell death compared to free Pt(IV), demonstrating the excellent chemosensitization of mCuPt 4T1 (Fig. 4b). To explore its ability to reverse cisplatin resistance, cisplatin-resistant A549R cells were incubated with CuPt and mCuPt for 24 h, and cell viability was measured using the MTT assay. Both mCuPt A549R and CuPt effectively induced A549R cell death, with mCuPt A549R exhibiting stronger inhibition of cell viability

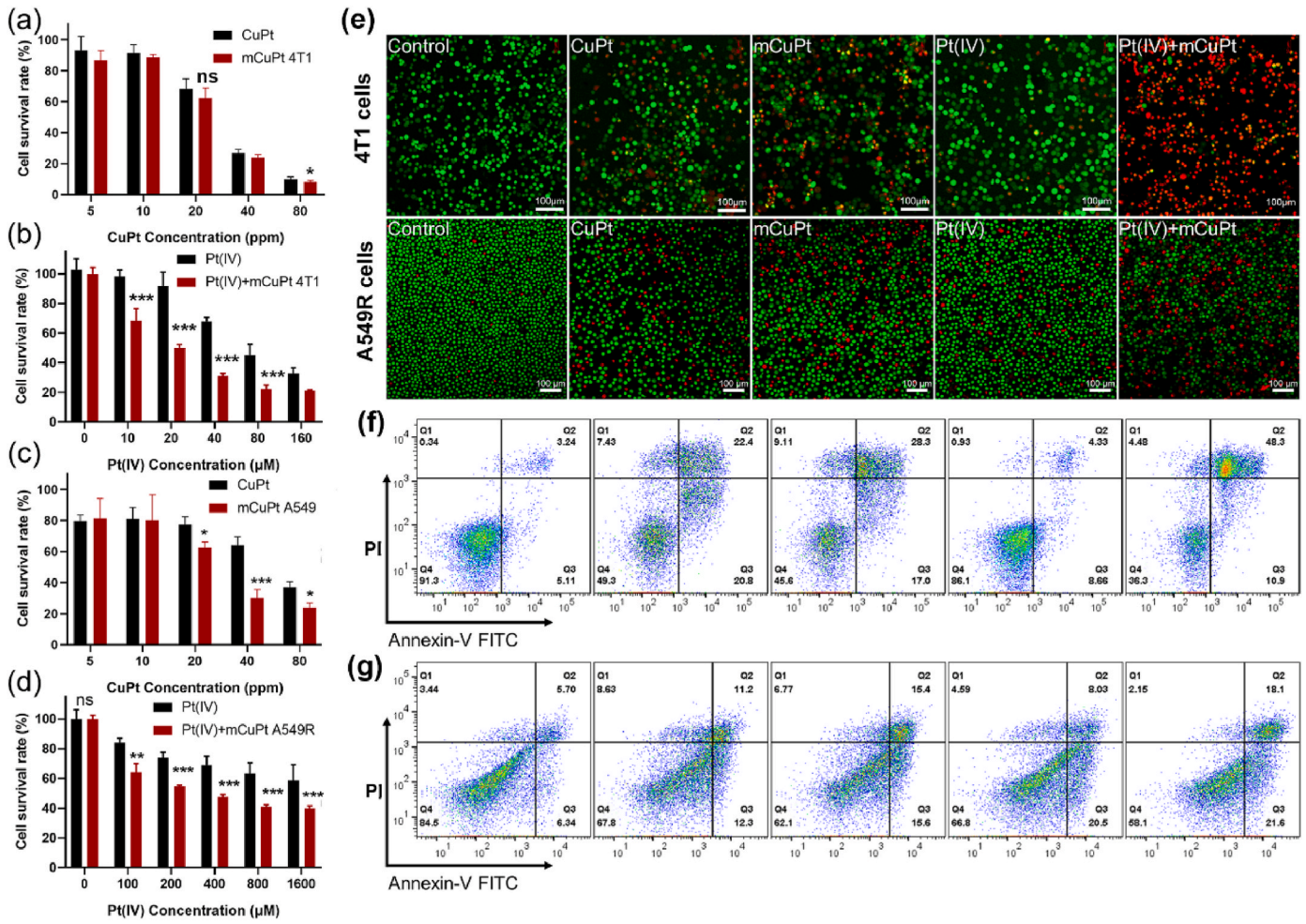

Fig. 4. Cytotoxicity assay of mCuPt 4T1 and mCuPt A549R. Viability of (a, b) 4T1 cells and (c, d) A549R cells treated by different groups; (e) Calcein-AM and PI staining of 4T1 cells and A549R cells treated with different groups; Flow cytometry apoptosis analysisof (f) 4T1 cells and (g) A549R cells treated with different groups.

than CuPt (Fig. 4c), suggesting excellent anticancer activity against cisplatin-resistant A549R cells. Impressively, mCuPt A549R significantly enhanced the sensitivity of A549R cells to the Pt(IV) prodrug, indicating efficient reversal of cisplatin resistance (Fig. 4d). Live and dead cell staining further confirmed the chemosensitization activity of mCuPt. As shown in Fig. 4e, the group treated with Pt(IV) alone induced minimal cell death, while the group treated with Pt(IV) plus mCuPt killed a greater number of cancer cells, consistent with the MTT results. Flow cytometric analysis of cell apoptosis yielded similar findings (Fig. 4f and g). Based on these analyses, it can be concluded that mCuPt not only effectively induces cancer cell death, but also enhances the chemosensitization of the Pt(IV) prodrug and reverses cisplatin resistance in tumor cells.

2.5. Action mechanism of mCuPt nanozyme-sensitized cell death

The mechanism by which mCuPt enhances Pt(IV) chemotherapy was further investigated. As previously mentioned, mCuPt exhibits strong POD-like activity, which may activate intracellular ROS. To monitor intracellular ROS production before and after mCuPt incubation, the fluorescence probe 2′,7′-dichlorofluorescin diacetate (DCFH-DA) was used. As depicted in Fig. 5a and e, the green fluorescence of A549R and 4T1 cells treated with mCuPt A549R and mCuPt 4T1 cells significantly increased, indicating the highest ROS production compared to other groups. Flow cytometry results also supported this observation, showing the strongest green fluorescence in the mCuPt group (Fig. 5b and f). Considering that excessive ROS induces depolarization of the mitochondrial membrane potential (Δψ, MMP), the JC-1 dye was employed to observe changes in MMP in cancer cells. As demonstrated in Fig. 5c and g, the ratio of red fluorescence to green fluorescence in A549R and 4T1 cells treated with mCuPt A549R and mCuPt 4T1 cells significantly decreased, indicating a reduction in MMP in cancer cells. Furthermore, western blotting (WB) analyzed the expression of mitochondria apoptosis-related proteins, including Bcl-2 and Bax, after different treatments (Fig. S11). The results indicated that the expression of Bax in both two cell lines treated with mCuPt significantly increased, while the expression of Bcl-2 decreased. Notably, the combination of mCuPt and the Pt(IV) prodrug induced the largest variation in Bcl-2 and Bax protein expression compared to single administration. These findings demonstrate that mCuPt effectively induces intracellular ROS production, leading to mitochondrial damage and ultimately resulting in cancer cell apoptosis.

Moreover, the previous studies reported that hypoxic tumor microenvironment was closely associated with tumor resistance. Therefore, relieving hypoxia has been proposed as a viable strategy to overcome chemoresistance. The mCuPt nanozyme, which exhibits excellent CAT-like activity, efficiently converts endogenous H_2O_2 into O_2, thereby alleviating tumor hypoxia. In order to assess the impact of mCuPt treatment on tumor hypoxia, we utilized the $[Ru(dpp)_3]Cl_2$ (RDPP) probe. As depicted in Fig. 5d and h, both A549R cells and 4T1 cells displayed intense red fluorescence naturally. Notably, the red fluorescence of both 4T1 cells and A549R cells treated with mCuPt 4T1

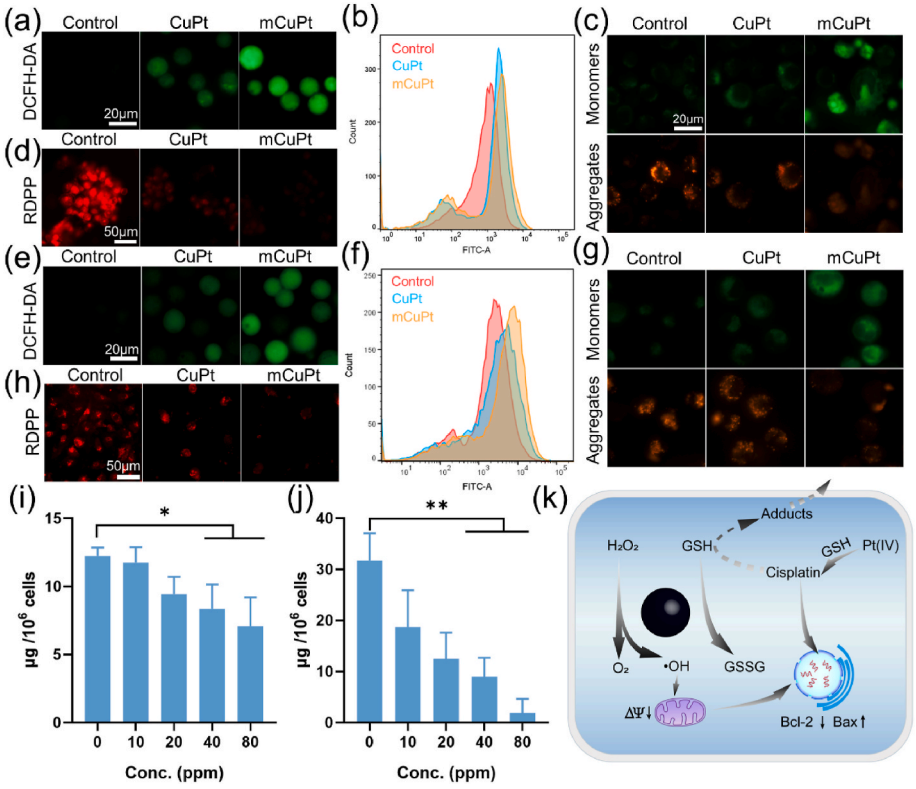

Fig. 5. Anticancer mechism assay of mCuPt 4T1 and mCuPt A549R *in vitro*. CLSM observation for intracellular (a, e) ROS detection by the DCFH-DA probe, (c, g) MMP detection by the JC-1 probe, (d, h) hypoxia detection by the RDPP probe; (b, f) Flow cytometry for intracellular ROS; (i, j) GSH detection of 4T1 cells and A549R cells treated with different samples, respectively; (k) The schematic diagram of GSH depletion, hypoxia relief, and ROS production induced by mCuPt.

nanozymes and mCuPt A549R nanozymes, respectively nearly disappeared, signifying a significant relief of tumor hypoxia. Moreover, the level of cellular GSH is an important determinant of cisplatin resistance in cancer cells. Generally, cellular GSH actively interacts with exogenous cisplatin, forming GSH-Pt adducts that are readily expelled by cancer cells, resulting in inefficient chemotherapy. Therefore, reducing GSH levels is essential for enhancing the efficacy of cisplatin chemotherapy. Subsequently, we investigated the ability of mCuPt to deplete cellular GSH using a GSH detection kit. As demonstrated in Fig. 5i and j and Fig. S12, mCuPt effectively consumed GSH in a dose-dependent manner, thereby minimizing interference with cisplatin and concurrently augmenting intracellular oxidative stress. Based on the aforementioned analysis, we conclude that mCuPt efficiently alleviates tumor hypoxia and depletes cellular GSH, thereby promoting the reversal of cisplatin resistance in tumors (Fig. 5k).

2.6. *In vivo antitumor activity of mCuPt-sensitized chemotherapy*

Encouraged by the impressive anticancer activity of mCuPt *in vitro*, we proceeded to evaluate its potential for enhancing chemotherapy and reversing cisplatin resistance *in vivo*. Initially, cisplatin-resistant A549R cells were subcutaneously inoculated into the right leg of nude mice to establish an A549R tumor model. Once the tumor volume reached 50 mm^3, the mice were randomly divided into five groups and administered with Saline, CuPt, mCuPt A549R, Pt(IV) and mCuPt A549R plus Pt(IV) prodrug at a dosage of 4 mg/kg (equivalent to CuPt), respectively. Then, the tumor volume and body weight of the A549R tumor-bearing mice were monitored every two days within the 14-day medication (Fig. 6a). The body weights of mice displayed negligible fluctuation during the therapeutic period, suggesting the good biosafety of mCuPt A549R (Fig. 6b). As shown in Fig. 6c, Pt(IV) prodrug was hard to inhibit tumor growth, which was attributed to the cisplatin resistance of the tumor. In addition, the slight suppression on tumor volume was observed in the mCuPt A549R treated group, whereas the combined administration of mCuPt A549R and Pt(IV) prodrug resulted in significantly smaller tumor volumes compared to the other groups. At the end of the treatment, the mice bearing A549R tumors were sacrificed, and the tumors and vital organs were dissected, photographed, and weighed. As shown in Fig. 6d and e, the combined therapy of mCuPt A549R and Pt(IV) prodrug exhibited the lowest weight and smallest size, demonstrating excellent tumor inhibition capability against cisplatin-resistant A549R tumors. In conclusion, mCuPt A549R effectively enhanced the chemosensitization of Pt(IV) prodrug, reversed cisplatin resistance, and ultimately achieved an outstanding anticancer effect.

Subsequently, the tumor sections were used for hematoxylin and eosin (H&E) staining, immunohistochemistry (IHC) staining, and fluorescence staining (Fig. 6f). The H&E results indicated modest variation in nucleus morphology in the single administration group, whereas the combination of mCuPt A549R and Pt(IV) prodrug effectively induced nucleus shrinkage and fragmentation, indicating significant tumor necrosis. Accordingly, mCuPt A549R plus Pt(IV) prodrug-treated group exhibited the lowest expression compared to the other groups, demonstrating stronger inhibition of tumor cell proliferation. Additionally, the ROS level in the tumor was analyzed using dihydroethidium (DHE) probe staining. Both the CuPt- and mCuPt-treated groups exhibited visible red fluorescence signals, indicating ROS production in the tumor tissue. As expected, a massive ROS signal was observed in the mCuPt A549R plus Pt(IV) prodrug-treated group, demonstrating the synergistic action of ROS-mediated tumor therapy.

2.7. *In vivo biosafety of mCuPt nanozymes*

Aside from the *in vivo* therapeutic effects, it was also an important consideration for assessing the biocompatibility, pharmacokinetics, and biodistribution of mCuPt. Initially, the CuPt nanoalloy and mCuPt were labeled with indocyanine green (ICG), and then the second near-infrared

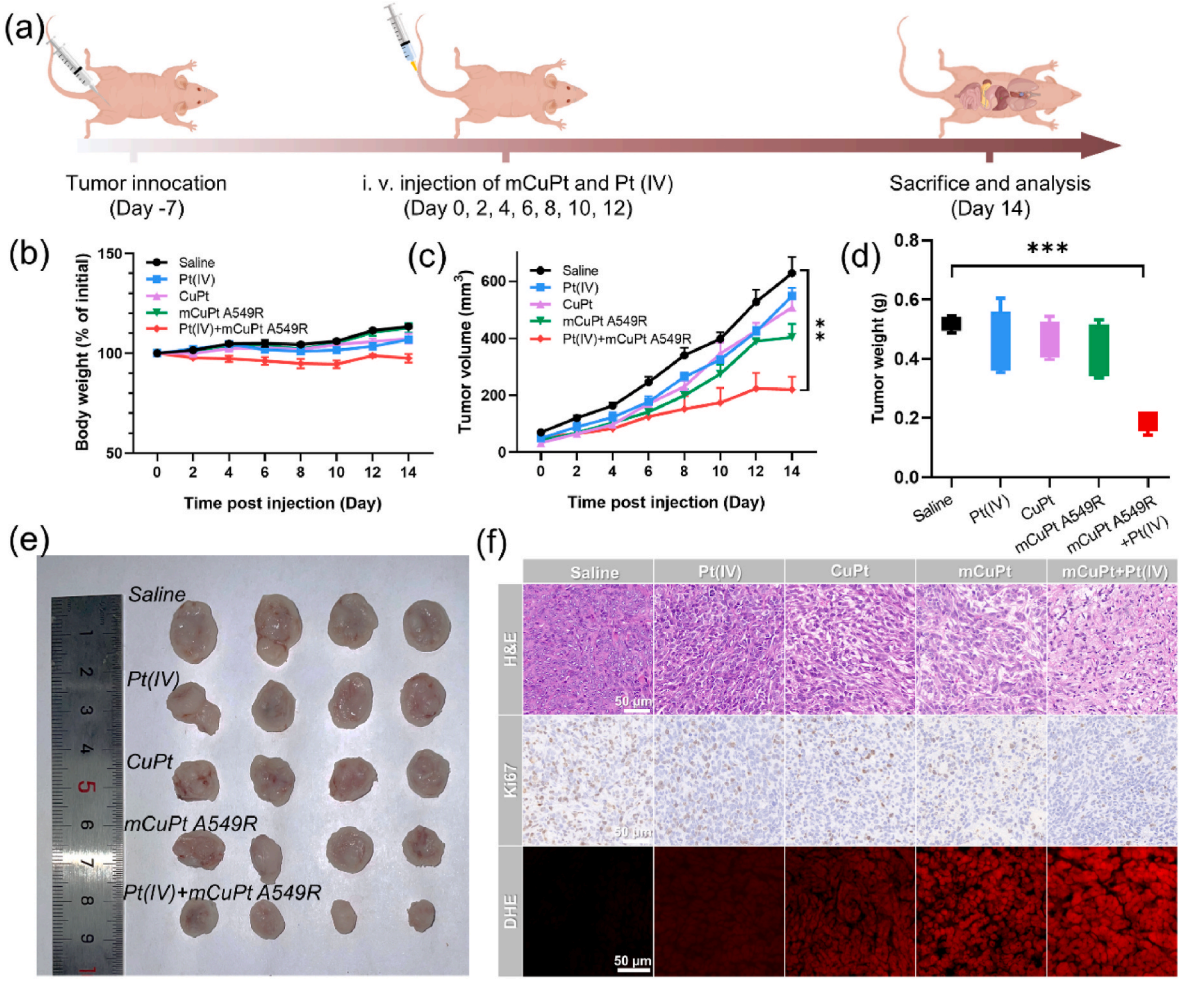

Fig. 6. *In vivo* antineoplastic assessment. (a) Diagram for *in vivo* therapeutic process; (b) Body weight change of mice treated with different groups; (c) Tumor volume changes and (d) tumor weight of mice treated with different groups; (e) Digital graphs of extracted tumors after different groups treatment; (f) H&E-, Ki67-and DHE-staining of tumor slice after different groups treatment.

(NIR-II) fluorescence imaging was performed to observe tumor accumulation and tissue distribution. As shown in Fig. 7a, the tumor of the mice injected with mCuPt exhibited a stronger signal at 48 h post injection compared to the CuPt treated group, indicating a homogeneous targeting effect. Additionally, biodistribution analysis revealed that the fluorescence signal was primarily observed in the liver, kidney, and tumor at 72 h post injection, suggesting that mCuPt could be excreted from the body. Pharmacokinetic analysis indicated that mCuPt had slightly prolonged blood circulation compared to CuPt, further confirming its complete excretion from the body. This result suggests that mCuPt not only enhanced tumor therapy but also avoided long-term toxicity in the body (Fig. 7b). Subsequently, the hemolysis assay and blood routine analysis were conducted to validate the hemocompatibility of mCuPt. It could be seen that both mCuPt and CuPt at various concentrations did not damage red blood cells (Fig. 7c). Additionally, the blood routine analysis indicated that all indices were within normal ranges at 48 h post-injection of CuPt and mCuPt, indicating negligible acute toxicity (Fig. 7d). These results demonstrate excellent hemocompatibility of mCuPt. Furthermore, H&E staining of vital organ sections (heart, liver, spleen, lung, and kidney) showed no significant histopathological variations after various treatments, demonstrating excellent tissue biosafety (Fig. 7e). Overall, mCuPt effectively enhanced the chemosensitization of Pt(IV) prodrug, reversed cisplatin resistance in tumors, and efficiently minimized systemic toxicity.

3. Conclusion

In summary, we successfully developed a cancer cell membrane-camouflaged CuPt nanozyme (mCuPt) to improve the sensitivity of Pt (IV) prodrug, enhance the anticancer effect, and reverse cisplatin resistance. The CuPt nanoalloy exhibited multiple enzyme-like activities, including POD-like, CAT-like, and GSHOx-like actions. The mCuPt accurately recognized tumors via homologous targeting effects and catalyzed endogenous H_2O_2 into •OH and O_2, thereby increasing tumor oxidative stress and relieving tumor hypoxia, respectively. Furthermore, mCuPt scavenged cellular GSH, reducing the inactivation of cisplatin drug. Cell assays demonstrated that mCuPt significantly enhanced the cytotoxicity of Pt(IV) prodrug, indicating excellent chemosensitization action. Moreover, in *in vitro* and *in vivo* experiments, the combination of mCuPt and Pt(IV) prodrug effectively inhibited cisplatin-resistant A549 cell proliferation and tumor growth, demonstrating its outstanding ability to reverse cisplatin resistance in tumors. This work highlights a promising strategy for overcoming cisplatin resistance by constructing a biomimetic multifunctional nanocatalytic system.

CRediT authorship contribution statement

Yuehao Gan: Data curation, Formal analysis, Investigation, Methodology, Resources, Software, Supervision. **Wenteng Xie:** Data curation, Formal analysis, Resources, Software, Supervision, Validation. **Miaomiao Wang:** Data curation, Formal analysis, Methodology, Project

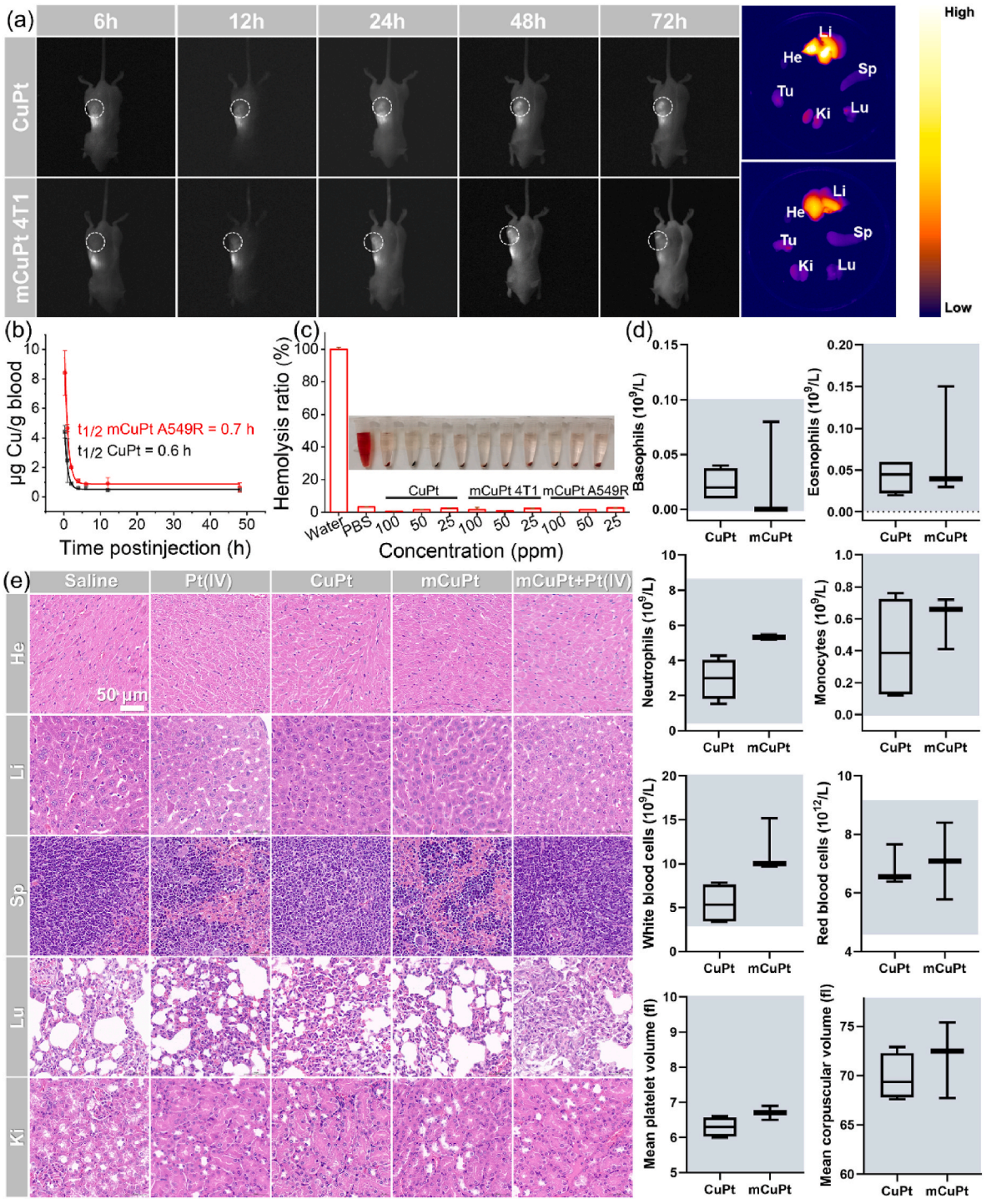

Fig. 7. Biosafety assessment of CuPt and mCuPt. (a) Tumor accumulation and biodistribution of CuPt and mCuPt; (b) Pharmacokinetics assay and (c) hemolysis analysis of CuPt and mCuPt; (d) The blood routine analysis of mice treated with CuPt and mCuPt (the normal range is within the grey area); (e) H&E-staining of main organ slice from different groups.

administration, Validation. **Peng Wang:** Resources, Software, Supervision. **Qingdong Li:** Formal analysis, Investigation, Methodology. **Junjie Cheng:** Resources, Software, Visualization. **Miao Yan:** Formal analysis, Investigation, Project administration. **Jikai Xia:** Conceptualization, Data curation, Formal analysis, Writing – original draft. **Zhengyan Wu:** Conceptualization, Data curation, Funding acquisition, Investigation, Project administration, Writing – review & editing. **Guilong Zhang:** Conceptualization, Data curation, Funding acquisition, Supervision, Validation, Visualization, Writing – original draft, Writing – review & editing.

Declaration of competing interest

The authors declare that they have no known competing financial interests or personal relationships that could have appeared to influence the work reported in this paper.

Data availability

Data will be made available on request.

Acknowledgements

A portion of this work was performed on the Steady High Magnetic Field Facilities, High Magnetic Field Laboratory, CAS. The authors would like to thank Shiyanjia Lab (www.shiyanjia.com) for the element mapping analysis. This work was supported by Key R&D Program of Shandong Province, China (No. 2023CXPT012); the National Natural Science Foundation of China (No. 22007006); Taishan Scholars Construction Engineering (No. tsqn201909144); Natural Science Foundation of Shandong Province (Nos. ZR2020QB102, ZR2021QH315).

Appendix A. Supplementary data

Supplementary data to this article can be found online at https://doi.org/10.1016/j.mtbio.2023.100941.

References

[1] B. Rosenberg, L. Vancamp, J. Trosko, V. Mansour, Platinum compounds: a new class of potent antitumour agents, Nature 222 (5191) (1969) 385–386.
[2] S. Rottenberg, C. Disler, P. Perego, The rediscovery of platinum-based cancer therapy, Nat. Rev. Cancer 21 (1) (2021) 37–50.
[3] Z. Wang, N. Wang, S. Cheng, K. Xu, Z. Deng, S. Chen, Z. Xu, K. Xie, M. Tse, P. Shi, H. Hirao, C. Ko, G. Zhu, Phorbiplatin, a highly potent Pt(IV) antitumor prodrug that can be controllably activated by red light, Chem 5 (12) (2019) 3151–3165.
[4] L. Amable, Cisplatin resistance and opportunities for precision medicine, Pharmacol. Res. 106 (2016) 27–36.
[5] M. Chovanec, M. Abu Zaid, N. Hanna, N. El-Kouri, L.H. Einhorn, C. Albany, Long-term toxicity of cisplatin in germ-cell tumor survivors, Ann. Oncol. 28 (11) (2017) 2670–2679.
[6] C. Tang, M. Livingston, R. Safirstein, Z. Dong, Cisplatin nephrotoxicity: new insights and therapeutic implications, Nat. Rev. Nephrol. 19 (1) (2023) 53–72.
[7] C. Jia, G. Deacon, Y. Zhang, C. Gao, Platinum(IV) antitumor complexes and their nano-drug delivery, Coord. Chem. Rev. 429 (2021) 213640.
[8] T. Johnstone, K. Suntharalingam, S. Lippard, The next generation of platinum drugs: targeted pt(II) agents, Nanoparticle Delivery, and Pt(IV) Prodrugs, Chem. Rev. 116 (5) (2016) 3436–3486.
[9] S. Tian, J. Li, D. Xiao, D. Ma, Self-enhanced catalytic activity of Pt/TiO_2 via electronic metal-support interaction, ACS Cent. Sci. 9 (1) (2023) 7–9.
[10] X. Zeng, Y. Wang, J. Han, W. Sun, H. Butt, X. Liang, S. Wu, Fighting against drug-resistant tumors using a dual-responsive Pt(IV)/Ru(II) bimetallic polymer, Adv. Mater. 32 (43) (2020) 2004766.
[11] X. Ling, X. Chen, I. Riddell, W. Tao, J. Wang, G. Hollett, S. Lippard, O. Farokhzad, J. Shi, J. Wu, Glutathione-scavenging poly(disulfide amide) nanoparticles for the effective delivery of Pt(IV) prodrugs and reversal of cisplatin resistance, Nano Lett. 18 (7) (2018) 4618–4625.
[12] G. Yang, Z. Pan, D. Zhang, Q. Cao, L. Ji, Z. Mao, Precisely assembled nanoparticles against cisplatin resistance via cancer-specific targeting of mitochondria and imaging-guided chemo-photothermal therapy, ACS Appl. Mater. Interfaces 12 (39) (2020) 43444–43455.
[13] Z. Chen, F. Han, Y. Du, H. Shi, W. Zhou, Hypoxic microenvironment in cancer: molecular mechanisms and therapeutic interventions, Signal Transduct. Target. Ther. 8 (1) (2023) 70.
[14] X. Jing, F. Yang, C. Shao, K. Wei, M. Xie, H. Shen, Y. Shu, Role of hypoxia in cancer therapy by regulating the tumor microenvironment, Mol. Cancer 18 (1) (2019) 157.
[15] H. Lin, Y. Chen, J. Shi, Nanoparticle-triggered in situ catalytic chemical reactions for tumour-specific therapy, Chem. Soc. Rev. 47 (6) (2018) 1938–1958.
[16] X. Lu, S. Gao, H. Lin, J. Shi, Single-atom catalysts for nanocatalytic tumor therapy, Small 17 (16) (2021) 2004467.
[17] J. Yang, H. Yao, Y. Guo, B. Yang, J. Shi, Enhancing tumor catalytic therapy by co-catalysis, Angew. Chem.-Int. Edit. 61 (17) (2022) e202200480.
[18] L. Gao, J. Zhuang, L. Nie, J. Zhang, Y. Zhang, N. Gu, T. Wang, J. Feng, D. Yang, S. Perrett, X. Yan, Intrinsic peroxidase-like activity of ferromagnetic nanoparticles, Nat. Nanotechnol. 2 (9) (2007) 577–583.
[19] M. Zandieh, J. Liu, Nanozymes: definition, activity, and mechanisms, Adv. Mater. (2023) 2211041.
[20] Z. Chen, Y. Yu, Y. Gao, Z. Zhu, Rational design strategies for nanozymes, ACS Nano 17 (14) (2023) 13062–13080.
[21] C. Peng, R. Pang, J. Li, E. Wang, Current advances on the single-atom nanozyme and its bioapplications, Adv. Mater. (2023) 2211724.
[22] L. Zhang, H. Wang, X. Qu, Biosystem-inspired engineering of nanozymes for biomedical applications, Adv. Mater. (2023) 2211147.
[23] M. Chang, Z. Hou, M. Wang, C. Yang, R. Wang, F. Li, D. Liu, T. Peng, C. Li, J. Lin, Single-atom Pd nanozyme for ferroptosis-boosted mild-temperature photothermal therapy, Angew. Chem.-Int. Edit. 60 (23) (2021) 12971–12979.
[24] J. Cheng, L. Li, D. Jin, Y. Dai, Y. Zhu, J. Zou, M. Liu, W. Yu, J. Yu, Y. Sun, X. Chen, Y. Liu, Boosting ferroptosis therapy with iridium single-atom nanocatalyst in ultralow metal content, Adv. Mater. 35 (17) (2023) 2210037.
[25] S. Somerville, Q. Li, J. Wordsworth, S. Jamali, M. Eskandarian, R. Tilley, J. Gooding, Approaches to improving the selectivity of nanozymes, Adv. Mater. (2023) 2211288.
[26] M. Lyu, M. Luo, J. Li, O. Akakuru, X. Fan, Z. Cao, K. Fan, W. Jiang, Personalized carbon monoxide-loaded biomimetic single-atom nanozyme for ferroptosis-enhanced FLASH radioimmunotherapy, Adv. Funct. Mater. (2023) 2306930.
[27] Y. Qi, Y. Chen, T. Xia, I. Lynch, S. Liu, Extra-pulmonary translocation of exogenous ambient nanoparticles in the human body, ACS Nano 17 (1) (2023) 12–19.
[28] J. Zhou, D. Xu, G. Tian, Q. He, X. Zhang, J. Liao, L. Mei, L. Chen, L. Gao, L. Zhao, G. Yang, W. Yin, G. Nie, Y. Zhao, Coordination-driven self-assembly strategy-activated Cu single-atom nanozymes for catalytic tumor-specific therapy, J. Am. Chem. Soc. 145 (7) (2023) 4279–4293.
[29] J. Liu, Y. Yuan, Y. Cheng, D. Fu, Z. Chen, Y. Wang, L. Zhang, C. Yao, L. Shi, M. Li, C. Zhou, M. Zou, G. Wang, L. Wang, Z. Wang, Copper-based metal-organic framework overcomes cancer chemoresistance through systemically disrupting dynamically balanced cellular redox homeostasis, J. Am. Chem. Soc. 144 (11) (2022) 4799–4809.
[30] J. Li, J. Zhang, X. Jiao, J. Shi, J. Ye, K. Song, J. Bao, G. Li, K. Lei, NIR-driven PtCu-alloy nanocages via photothermal enhanced fenton catalytic degradation of pollutant dyes under neutral pH, J. Alloy. Compd. 895 (2022) 162624.
[31] C. Wu, R. Li, Y. Wang, S. Lu, J. Lin, Y. Liu, X. Zhang, Strong metal-support interactions enable highly transparent Pt-Mo_2C counter electrodes of bifacial dye-sensitized solar cells, Chem. Commun. 56 (69) (2020) 10046–10049.
[32] T. Chen, G. Han, X. Li, Platinum-copper alloy nanoparticles armored with chloride ion transporter to promote electro-driven tumor inhibition, Bioact. Mater. 12 (2022) 143–152.
[33] X. Zhong, X. Wang, L. Cheng, Y. Tang, G. Zhan, F. Gong, R. Zhang, J. Hu, Z. Liu, X. Yang, GSH-depleted $PtCu_3$ nanocages for chemodynamic-enhanced sonodynamic cancer therapy, Adv. Funct. Mater. 30 (4) (2020) 1907954.
[34] Z. Wang, R. Zhang, X. Yan, K. Fan, Structure and activity of nanozymes: inspirations for de novo design of nanozymes, Mater. Today 41 (2020) 81–119.
[35] B. Yu, W. Wang, W. Sun, C. Jiang, L. Lu, Defect engineering enables synergistic action of enzyme-mimicking active centers for high-efficiency tumor therapy, J. Am. Chem. Soc. 143 (23) (2021) 8855–8865.
[36] Y. Zhu, R. Zhao, L. Feng, C. Wang, S. Dong, M.V. Zyuzin, A. Timin, N. Hu, B. Liu, P. Yang, Dual nanozyme-driven PtSn bimetallic nanoclusters for metal-enhanced tumor photothermal and catalytic therapy, ACS Nano 17 (7) (2023) 6833–6848.